The Effect of the Mixing Region Geometry and Collector Distance on Microbubble Formation using a Microfluidic Device coupled with AC-DC Electric Fields

Anjana Kothandaraman *[1][¥], Yasir Alfadhl [2], Muhammad Qureshi [2], Mohan Edirisinghe [1], Yiannis Ventikos [1]

[1] Department of Mechanical Engineering, University College London, London WC1E 7JE, United Kingdom
[2] School of Electronic Engineering and Computer Science, Queen Mary University of London, London E1 4NS, United Kingdom

¥ Present address: Department of Mechanical Engineering, University of Birmingham, Birmingham B15 2TT, UK.

Corresponding author: A.Kothandaraman@bham.ac.uk
                       Tel: +44 121 414 4147

Abstract

In this work we report a significant advance in the preparation of monodisperse microbubbles using a combination of microfluidic and electric field technologies. Microbubbles have been employed in various fields such as biomedical engineering, water purification and food engineering. Many techniques have been investigated for their preparation. Of these, the microfluidic T-Junction has shown great potential due to the high degree of control it has over processing parameters and the ability to produce monodisperse microbubbles. Two main lines of investigation were conducted in this work – the effect of varying the mixing region distance (M_x) and the influence of altering the tip-to-collector distance (D_x) when an AC-DC field is applied. It was found that when M_x was decreased from 200µm to 100µm, the microbubble size also decreased from 128 ± 3 µm to 88 ± 5 µm due to an increase in shear stress as a result of a reduction in surface area. Similarly, decreasing the tip-to-collector distance results in an increase in electric field strength experienced at the nozzle, facilitating further reduction of bubble size from 111 ± 1 µm to 86 ± 1µm at an AC voltage of 6kV P-P and an applied DC voltage of 6kV. Experiments conducted with the optimal parameters identified from the previous experiments enabled further reduction of the microbubble size to 18 ± 2 µm. These results suggest that a unique combination of parameters can be employed to achieve particular microbubble sizes to suit various applications.

1. Introduction

Microbubbles are being increasingly used in a variety of key advanced technologies including food engineering, water purification and biosensing applications. Microbubbles play a vital role in the manufacturing of a plethora of food products such as: ice creams, beverages and cakes. Aeration of food also benefits from low costs and form novel structures that play a vital role in oral sensory perception [1]. Their versatility is incorporated in beverages to enhance the visual appeal of soft drinks, beers and wine [2]. They are also used as texture modifiers and fat replacers, which can potentially pave way for the development of healthier food products without compromising their taste [3-4]. Furthermore, substituting conventional microbubbles with microbubbles coated with nutritional ingredients or drugs can increase the nutritional value and introduce medicinal properties in food.

Their applications extend beyond the realm of food engineering into waste water treatment in processes such as ozonation and floatation [5-6]. Due to the steady decline in the availability of water resources, alternative procedures to obtain purified water, such as sea water desalination, have gained substantial interest [7]. Microbubbles have also been introduced into bioreactors to extract biogases such as methane in waste water [8]. The microbubbles provide a gas-liquid interface where the methane aggregates, thus providing a means to exit the system. Dissolved air flotation (DAF) employs microbubbles of diameters < 150μm to separate particulates from potable water by harnessing on their high surface area to volume ratio which improves the mass transfer rate[9]. Shu et al.[10] added that incorporating microbubbles into active sludge results in sludge flotation and accumulation at the surface. Consequently, there is a decrease in sludge volume in the main tank for subsequent eradication or purification processes [11]. Biosensors are used in food safety measurements to detect bacteria such as Escherichia Coli (E-Coli) due to their high level of sensitivity and accurate detection of harmful pathogens [12]. Recent developments indicate that gas microbubbles coated with an albumin, lipid, phospholipid or polymer shell influence the electroacoustic response of the microbubble, therefore being a feasible option for acoustic biosensing platforms [13].

In order to cater to the numerous applications, it is essential to have optimal control over the microbubble production process and tailor their diameter to suit specific applications. Microfluidic configurations have established their versatility in various fields for effective microbubble generation. Specifically, the use of a T-Junction device has been widely investigated due to the exquisite control it offers over processing parameters such as solution flow rate and gas pressure, which govern the dynamics of droplet formation and detachment at the junction. This device also benefits from low set-up costs, natural scalability and the convenience to replace capillaries in the event of blockage. Fluid flow in the capillaries is controlled by high precision mechanical pumps and gas pressure is controlled by adjusting the regulator on a gas tank. An ideal range and combination of parameters exist in order to attain the desired microbubble diameters to suit specific applications. At a constant liquid flow rate, minimum and maximum inlet gas pressures can be defined as P_{gmin} and P_{gmax} respectively[14]. Any pressure below P_{gmin} would cause the liquid stream to push the gas stream back up the capillary, as a result of the capillary force of the liquid. Increasing the pressure past P_{gmax} disturbs the overall laminar flow of both streams in the outlet capillary and pushes the liquid stream back into the liquid inlet capillary. The mixing of both fluid media takes place in the gap where the two inlet tubes meet which will be referred to herewith as the mixing region.

Gupta et al.[15] investigated the effect of altering the width and depth of junction capillaries on the bubble size. They studied the effect of manipulating the channels height (w_l) and width (w_c). When the emerging bubble blocks the main channel; obstruction of the channel causes an increase in

pressure upstream[16]. Due to the presence of interfacial tension retaining the curvature of the droplet, when w_c is increased; the pressure upstream needs to overcome a higher Laplace pressure difference denoted by:

$$\Delta P_L = \sigma \left(\frac{1}{R_a} + \frac{1}{R_r} \right) \tag{1}$$

where σ is the surface tension, R_a and R_r are the principal radii of curvature respectively[17]. The increased duration of time results in the emerging bubble filling a larger section of the channel. Once the pressure is sufficient to overcome the interfacial tension, the droplet neck pinches off forming a larger bubble. The opposite effect was observed with lower w_c.

Microbubble size reduction is limited under this small window of parameter manipulation, especially when viscous solutions are used. For this reason, the idea of merging electrohydrodynamics into the set-up was explored by introducing a DC electric field at the outlet capillary [18]. When an electric field is applied, electrical charge accumulates at the gas liquid interface, which behaves as a capacitor. As the voltage increases, the charge build up at the interface increases resulting in a higher attraction of the gas stream downstream. The resulting elongation of the gas column and radial compression accelerates the breakup process causing a reduction of bubble size which was also observed by Parhizkar et al.[18]. However, microbubble size reduction ceased at voltages above 12kV.

Another idea that has been explored in literature is the superimposition of an AC on a DC electric field [19-21] to generate liquid droplets by electrospraying. Jaworek et al. [19] indicated that this divides the waveform into two components – the AC and the DC. The DC component is applied by shifting the zero line up to a specific voltage, which acts as the new time base. The AC component is introduced as a waveform oscillating about this new time base at a (P-P) voltage. For instance, setting the DC voltage to 5kV with a superimposed AC voltage of 4kV $_{P-P}$, oscillates the waveform between 3kV and 7kV. Balachandran et al.[20] superimposed an AC on DC electric field to facilitate liquid droplet formation in their electrospraying apparatus. They noticed that increasing the frequency of the applied signal resulted in an increase in droplet formation rate and a subsequent decrease in droplet size suggesting that frequency is an important contributor to droplet break-up. Although the behaviour of a bubble subjected to oscillating fields has been investigated, preparation of bubbles has not been reported using this method.

Various experimental configurations have been employed to introduce an oscillating electric field to an electrospraying set-up and extensive research has been conducted on the various channel configurations. However, to the best of the authors' knowledge, oscillating electric fields have not been integrated into microfluidic arrangements and the effect of the separation gap between the gas inlet and the liquid inlet (referred to as Mx (figure 1b) herewith) has not been studied. In this work, a novel apparatus to superimpose an AC on DC electric field was utilised. We investigate the effect of varying M_x, followed by varying the distance between the ground collector and nozzle tip (D_x) when an oscillating electric field is introduced into the experimental set-up to identify optimal parameters to facilitate bubble size reduction.

2. Materials and Methods

Solutions

For simplicity, a model system comprising of bovine serum albumin (BSA) and water was used. BSA (molecular weight: 66000gmol^{-1}) was purchased from Sigma Aldrich (Poole, UK). Solutions of 10% w/w and 15% w/w were prepared by dissolving BSA in distilled water using magnetic stirrers for 24 hours.

Solution	Viscosity (mPa s)	Surface Tension (mN m^{-1})	Electrical Conductivity (μS m^{-1})	Relative permittivity at 25.3°C	Density (kg m³)
10% w/w BSA	1.0	56	5.00 x 10^6	67.3	1065
15% w/w BSA	1.6	51	6.44 x 10^6	81.5	1070

Table 1: Physical Properties of 15% BSA and 10% BSA

Characterisation of Solutions

The density of the solutions was measured using a 25ml DIN ISO 3507 Gay-Lussac type density bottle (VWR International, Lutterworth, UK). The viscosity was measured using an Ostwald Viscometer (Schott Instruments GmbH, Mainz, Germany). The surface tension of the solution was measured using a Wilhelmy Plate tensiometer (Kruss, Hamburg, Germany) and the electrical conductivity was studied using a Jenway 3540 conductivity meter (Bibby Scientific, Stone, UK). The dielectric properties of BSA 10% and 15% were measured using an open ended coaxial probe method combined with an Agilent network analyser. Measurements of the complex permittivity (ε*) comprising of both real and imaginary components i.e. ε' (relative permittivity), and ε" (loss factor) were carried out over the frequency band 0.4GHz up to 20GHz. The choice of the frequency band was influenced by the available measurement kit, however, the required properties at the desired lower frequencies were deduced from the measured values. The Cole-Cole model[22] was applied on the measured data by generating relaxation parameters at measured frequency range in order to predict the dielectric properties at low frequency range. The physical properties of the solutions used to prepare the microbubbles are summarised in table 1.

Experimental Set-up

Two experimental configurations were utilised in this work, one with and without an electric field. In order to introduce the superimposed AC on DC field, a waveform generator was used to drive the input of a High Voltage Amplifier (HVA) (Trek, Lockport, New York,USA) as shown in figure 1a[23]. This enables applying an offset to the output signal forming the DC component, and is coupled with a Peak-to-Peak (P-P) AC voltage. This resultant signal ranging from 0-10V is amplified to 0-10kV.
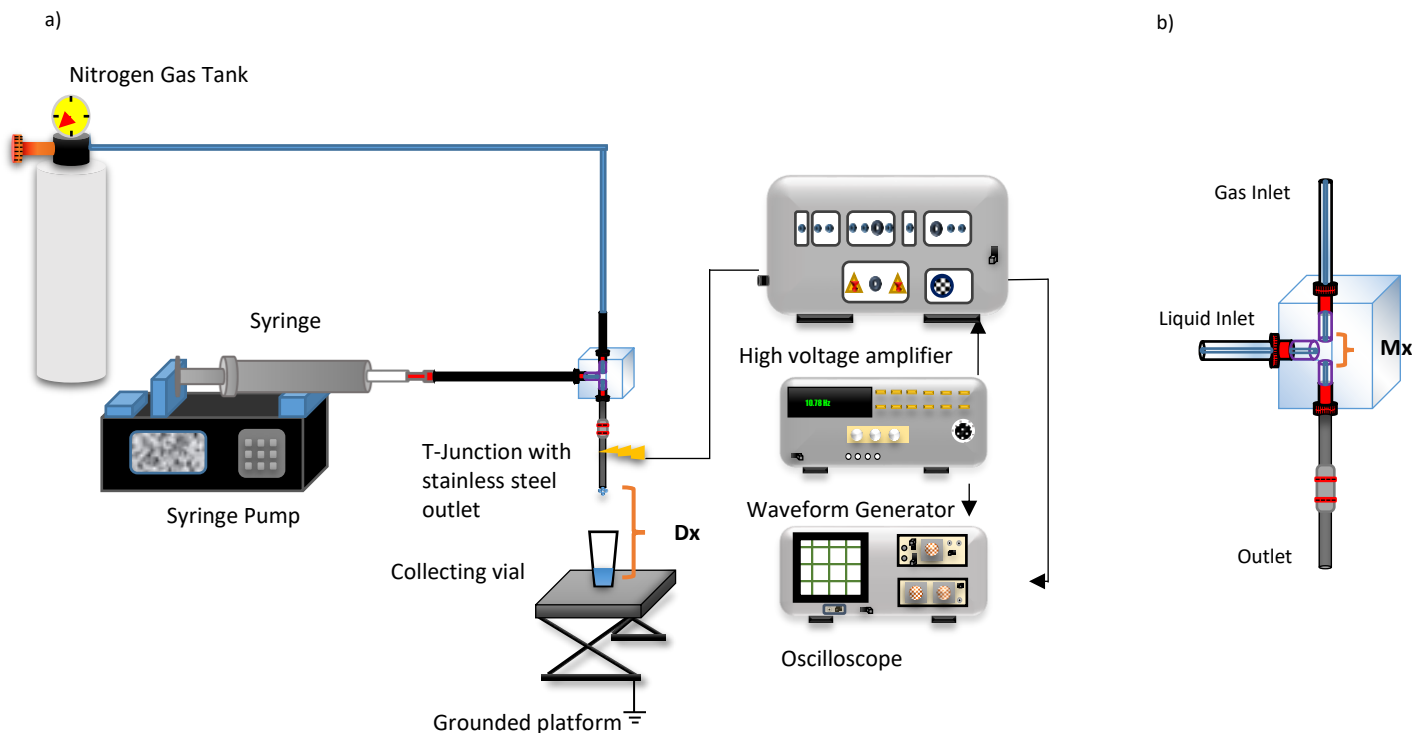
Figure 1: a) Experimental set-up to superimpose an AC on a DC electric field, indicating Dx, which is the distance between the nozzle tip and collector b) Schematic of T-junction indicating Mx

Bubble Generation

The first series of experiments were conducted using the T-Junction only in order to investigate the effect of varying the geometry of the mixing region on the bubble size. Two Fluorinated Ethylene Propylene (FEP) tubes of 100µm were arranged coaxially and a third FEP tube was connected perpendicular to the first pair, to form the T-Junction. The top inlet was connected to a pressurised gas tank containing nitrogen, and the second inlet was connected to a syringe holding the solution driven by a mechanical pump. The fluid was injected at a constant flowrate of 100µl/min and the gas was at a constant pressure of 256kPa. These two fluids meet at the junction area, where bubbles form, which traverse through the outlet capillary and are collected on a glass slide. The mixing region geometry was varied by altering the gap distance between the gas inlet and outlet capillary from 100µm-220µm. The superimposed electric field was introduced into the system by replacing the FEP tube outlet with a stainless steel outlet to provide a conductive surface. All experiments were conducted in cleanroom conditions under an ambient temperature of 20°C and a relative humidity of 40%. Supplementary information (1 and 2) illustrates bubble generation with and without the electric field, respectively.

Characterisation of Bubbles

Microbubbles were collected on a glass slide and observed under an optical microscope (Nikon Co, Tokyo, Japan) immediately after generation. The optical micrographs were studied using ImageJ 1.48v imaging software (National Institute of Health, Maryland, USA).

3. Results and Discussion

Effect of varying mixing region geometry

Many have investigated the effect of solution properties and various processing parameters on bubble formation previously; however not much relevance has been given to junction where both fluid media meet.
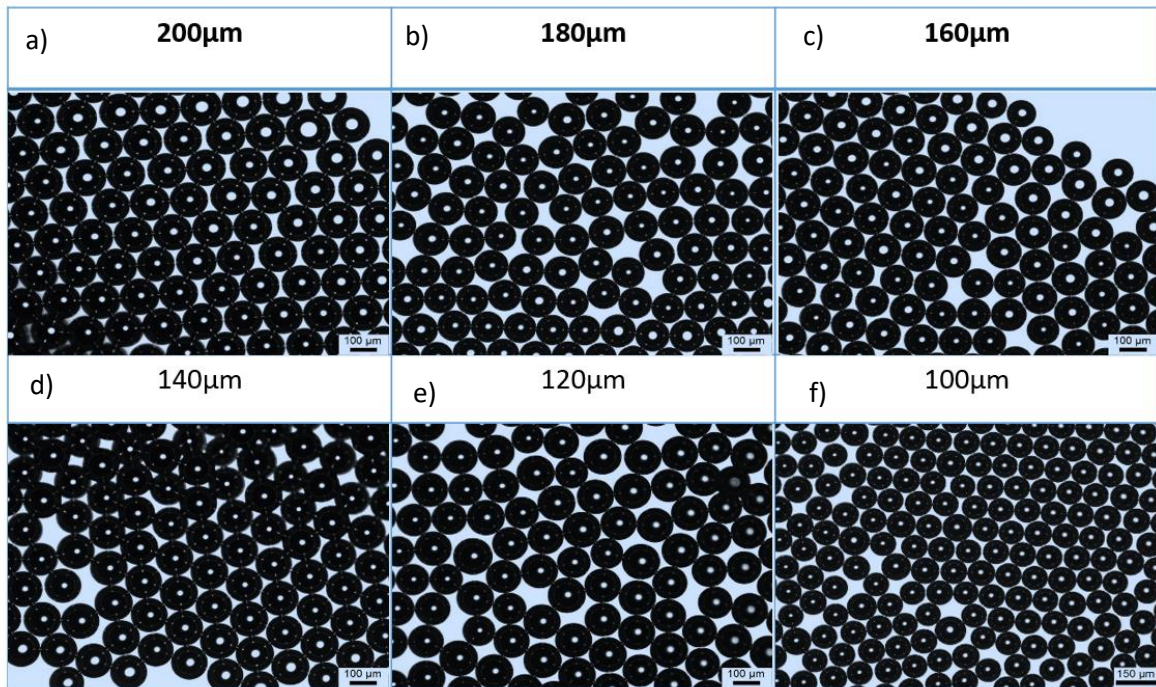

Figure 2: Optical Micrographs of bubbles of 15% BSA obtained at Mx of a) 200µm b) 180µm c) 160µm d) 140µm e) 120µm f) 100µm
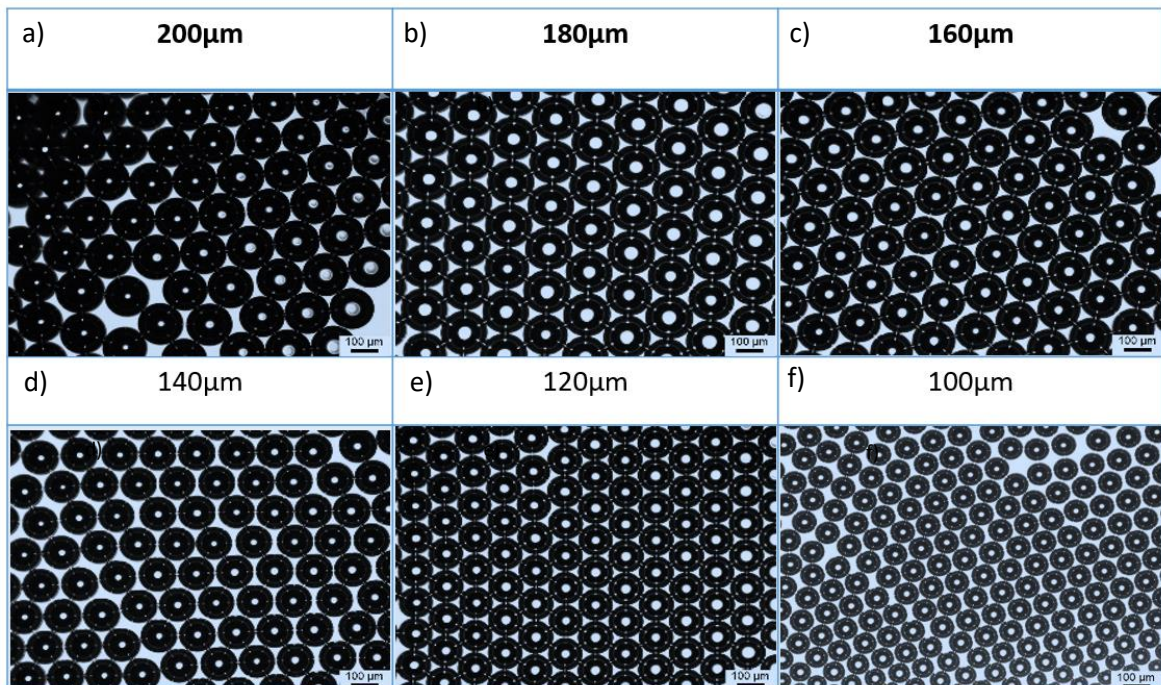

Figure 3: Optical Micrographs of bubbles of 10% BSA obtained at Mx of a) 200µm b) 180µm c) 160µm d) 140µm e) 120µm f) 100µm

The gap size was varied by altering the distance between the top inlet and the stainless steel capillary between 100µm-200µm. The effect of varying M_x on the bubble diameter was investigated using two different concentrations of BSA. The first series of experiments were conducted using 15% wt.

concentration of BSA. A constant gas pressure of 106.7kPa and a liquid flow rate of 130μl/min were retained for all values of M_x. Figure 2 displays optical micrographs of microbubbles collected at various Mx values; it can be observed that there is a constant and progressive decrease in diameter with decreasing M_x. The microbubbles produced at an Mx distance of 200μm were 128 ± 3μm, when Mx is reduced to 160μm, the bubble size was reduced to 98 ± 1μm. Setting the gap distance to 100μm, in line with the inner diameter of all the tubes accelerates reduction to yield microbubbles of 71 ± 4 μm. However, the FEP tubes were blocked, and had to be replaced frequently, due to the high viscosity of the 15% wt. BSA solution.

The experiments were repeated using a 10% wt BSA solution, the optical micrographs obtained at different values of Mx are shown in figure 3. Similar to the trend displayed in figure 2, a solution of 10% displays a more refined and steady decrease in bubble size as shown in figure 3. When Mx is reduced from 200μm to 140μm, a microbubble diameter reduction from 128 ± 2μm to 108 ± 1μm is observed. Setting the gap size to 100μm, promotes a further descent in bubble diameter to 88 ± 5μm. This reduction is not as steep in comparison with the 15% wt. BSA solution which has a higher viscosity than the latter.

Solutions of higher viscosities have shown to produce bubbles of smaller size in previous studies[14], which suggested that this was due the relative increase in the shear force over the capillary force at the channel junction. Microflows are characterised by low Reynolds numbers[24] for the liquid:

$$Re = \frac{Q_l \rho_l}{\mu_l D} \tag{2}$$

And for the gas:

$$Re = \frac{Q_g \rho_g}{\mu_g D} \tag{3}$$

where Q_l, ρ_l, μ_l, Q_g, ρ_g, μ_g and D are the volumetric flow rate of the liquid, liquid density, dynamic viscosity of the liquid, volumetric flowrate of the gas, gas density, dynamic viscosity of the gas and the hydraulic diameter of the capillaries respectively), hence the flow is laminar and the fluid flow is governed by viscous forces rather than inertial forces. This indicates that altering either gas pressure or liquid flow rate will have an impact on the bubble size. The FEP tubes utilised in these experiments have a hydraulic diameter of 100μm, Garstecki et al. [24] elaborated that for microchannels of this diameter, flows typically have very low capillary numbers ($Ca < 10^{-2}$):

$$Ca = \frac{\mu u}{\sigma} \tag{4}$$

where u is the average velocity of the continuous phase and σ is the interfacial tension; therefore the size of the bubbles produced is governed by the pressure balance between the gas and the liquid. The emerging droplet/slug occupies the entire channel geometry leading to an increase of pressure

upstream, which consequently leads to bubble growth and a generation of a neck where the bubble is trying to pinch off from the continuous phase. Baroud et al. [25] added that droplet break-up occurs when the viscous shear stress overcomes the surface tension that retains the curvature of the emerging bubble. This suggests that an increase in viscosity further increases this shear force at the junction area, thus resulting in the formation of smaller bubbles. Based on these theories, decreasing the value of Mx, consequently reduces the surface area which also results in an increase of the shear force across the mixing region in the junction contributing the formation of smaller bubbles. A summary of the bubble size with different values Mx for both concentrations of solution is shown in figure 4.
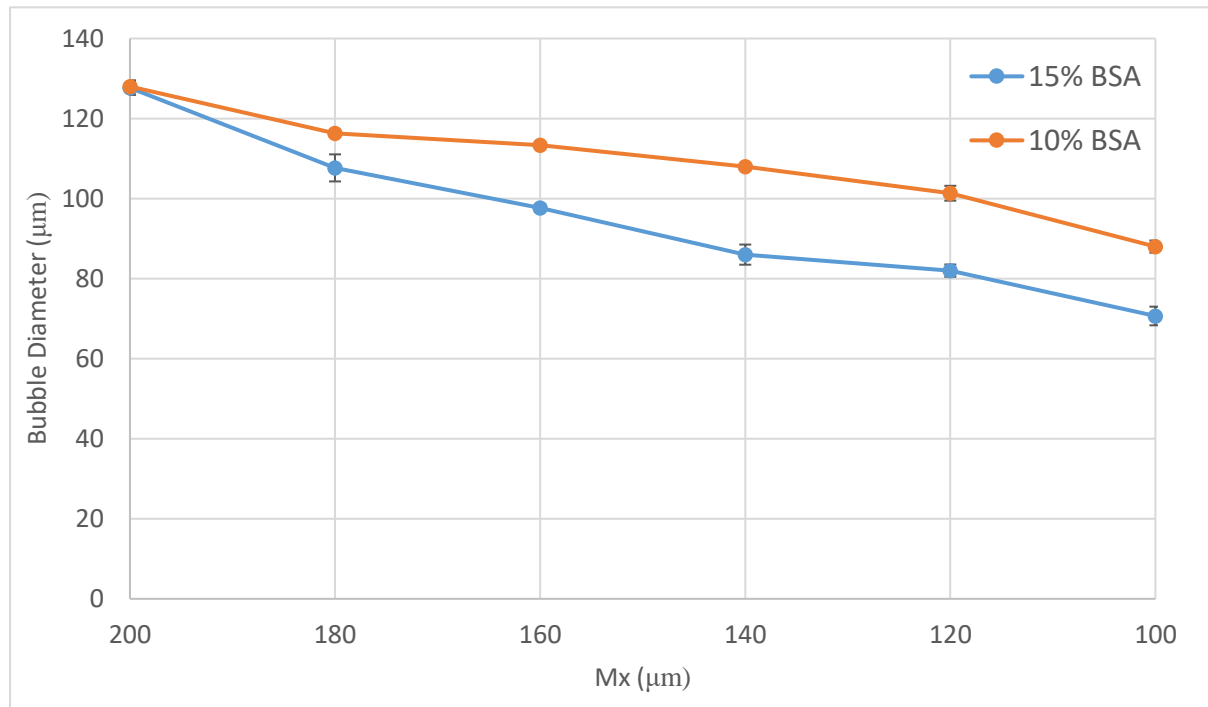

Figure 4: Graph of Bubble Diameter versus Mx for 15% wt. and 10% wt. Bovine Serum Albumin Solutions.

Although, utilising a solution of higher viscosity with a smaller Mx produced smaller bubbles, the capillaries were easily blocked hence required to be replaced regularly, as experienced by other researchers[14, 18, 26]. Therefore, it is essential to employ solutions of lower viscosities such that the liquid and air pressures required can be reduced[27]. These results indicate that to obtain microbubbles of ~60μm diameter without an external field employing a 10% wt. solution, the separation distance between the co-axially aligned capillary channels must be 100μm, which is the same as the internal diameter of all the capillary channels.

Effect of Varying Electric Field Strength

Bubble size reduction experiences limitations in experimental configurations without external electric fields. Electrohydrodynamic techniques have also been used to generate microbubbles using a dual needle configuration called coaxial electrohydrodynamic atomisation (CEHDA)[28]. This allows the formation of multi-layered bubbles, particles and capsules. Electrohydrodynamic theory encompasses the behaviour of a liquid stream when subjected to an electric field [29]. When the liquid stream reaches the nozzle, the hemispherical meniscus is held together by interfacial tension which Zeleny[29] described by the following equation:

$$\sigma = \frac{rh\rho g}{2} \qquad (5)$$

where *r* is the radius of the nozzle, *h* is the height of the liquid required to cause the hemispherical shape of the meniscus and g is the gravity constant. When an electric field is applied at the nozzle, the liquid is gradually charged up, and the electric field intensity (*f*) experienced at the liquid surface is given by:

$$f = \sqrt{8\pi x \rho g} \qquad (6)$$

where *x* is the length of the liquid column whose hydrostatic pressure counteracts the elongation caused by the electric field acting on the liquid surface. Once the electric field overcomes the interfacial tension, the meniscus releases a thin jet to produce fibres or breaks up to form fine droplets. Introducing an electric field in the form of a steady state DC constrained parameter manipulation to only variation of the applied voltage[18]. Parhizkar et al.[18] observed significant bubble reduction at very high voltages of 12kV. This may be due to the fact that the distance between the ground collector and the nozzle was too large, thus generating a lower electric field strength. We would like to add that this is limited to particular geometric configurations of the channels.

Another idea that has been explored in literature is superimposing an AC on a DC electric field [19-21, 30] and vary the amplitude of the AC . Depending on the applied frequency and amplitude, the bubbles are subjected to non-linear oscillations, which results in their break-up when further increased [31]. The electrospray system in conjunction with an AC/DC excitation was first proposed by Vonnegut and Neubauer [32]. They controlled the droplet formation process by an AC voltage of 60 Hz, and suggested that the use of pulsed DC electric fields can control the frequency of droplet formation.
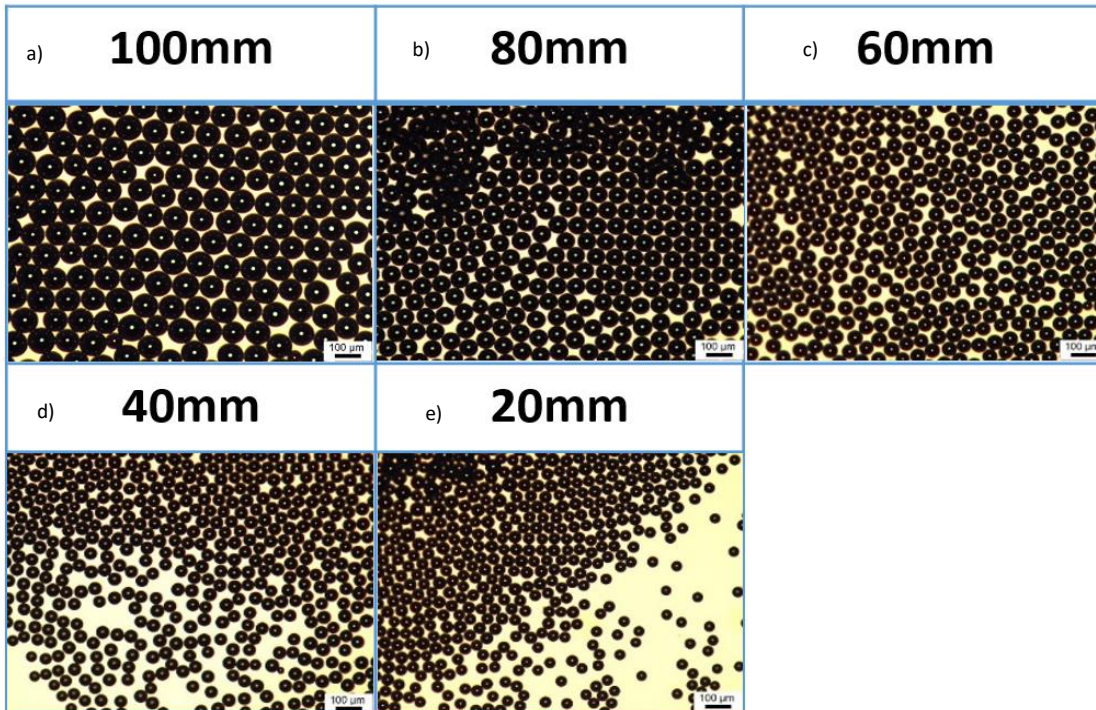

Figure 5: Effect of varying Dx at 6kV DC, 2kV AC P-P, 2kHz. A 10% BSA solution was used in the experiments, and Dx values are a) 100mm b) 80mm c) 60mm d) 40mm e) 20mm

We developed a novel experimental set-up that superimposes an AC on a DC electric field to facilitate microbubble break-up[23], further details can be found in the supplementary information provided. Using this configuration, the effect of varying the tip-to-collector distance (D_x) was investigated. The tests were conducted with two different applied DC voltages keeping the applied AC and frequency constant at different electric field strengths. Figure 5 displays optical micrographs of microbubbles obtained at 6kV DC, 2kV $_{(P-P)}$, 2kHz. The bubble size was observed to drastically reduce with decreasing (D_x). Reducing (D_x) from 100mm to 80mmm results in the average microbubble diameter decreasing from 110 ± 1μm to 101 ± 2μm, which further decreases to 86 ± 1μm when the electric field strength is 300,000 V/m (D_x = 20mm). A similar phenomenon was observed when the applied DC was increased to 8kV DC (figure 6) keeping the other parameters constant. The microbubble size decreased from 111 ± 1μm to 97 ± 2μm at a D_x value of 20mm. A roughly similar drop in bubble diameter was recorded at a (D_x) value of 80mm when 6kV DC was utilised. The results for 6kV DC and 8kV DC are summarised in figure 7.

A DC electric field strength of 100,000V/m can be achieved at 6kV and 8kV by setting the tip-collector distance to 60mm and 80mm respectively. The microbubble diameter decreased from 111± 1μm to 92 ± 2μm , displaying a 17% reduction in size with an absolute DC voltage magnitude of 6kV. On the other hand, a decrease in size from 111 ± 1μm to 106 ± 5μm was recorded at a DC voltage magnitude of 8kV displaying a 4% decrease. Similarly, at an electric field strength of 500,000 V/m requires Dx to be 12mm and 16mm at 6kV and 8kV respectively. A 23% decrease in the microbubble diameter was observed at 6kV and a 12% decrease at 8kV. These observations indicate that the variation in bubble size is partly influenced by the applied absolute DC voltage magnitude and the DC electric field strength. Smaller bubble sizes can be achieved at lower absolute DC voltage magnitudes by adjusting the tip-to-collector distance to increase the electric field strength.
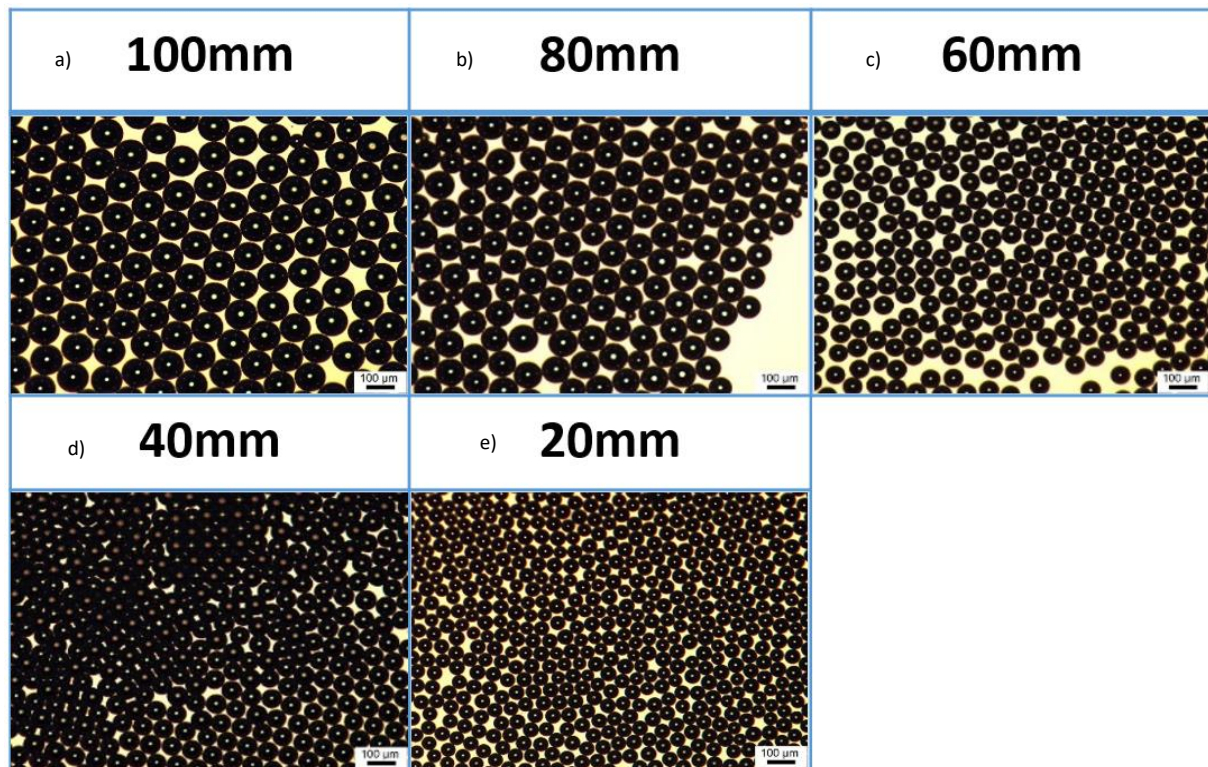

Figure 6: Effect of Dx at 8kV DC, 2kV AC P-P, 2kHz. A 10% BSA solution was used in the experiments, and Dx values are a) 100mm b) 80mm c) 60mm d) 40mm e) 20mm
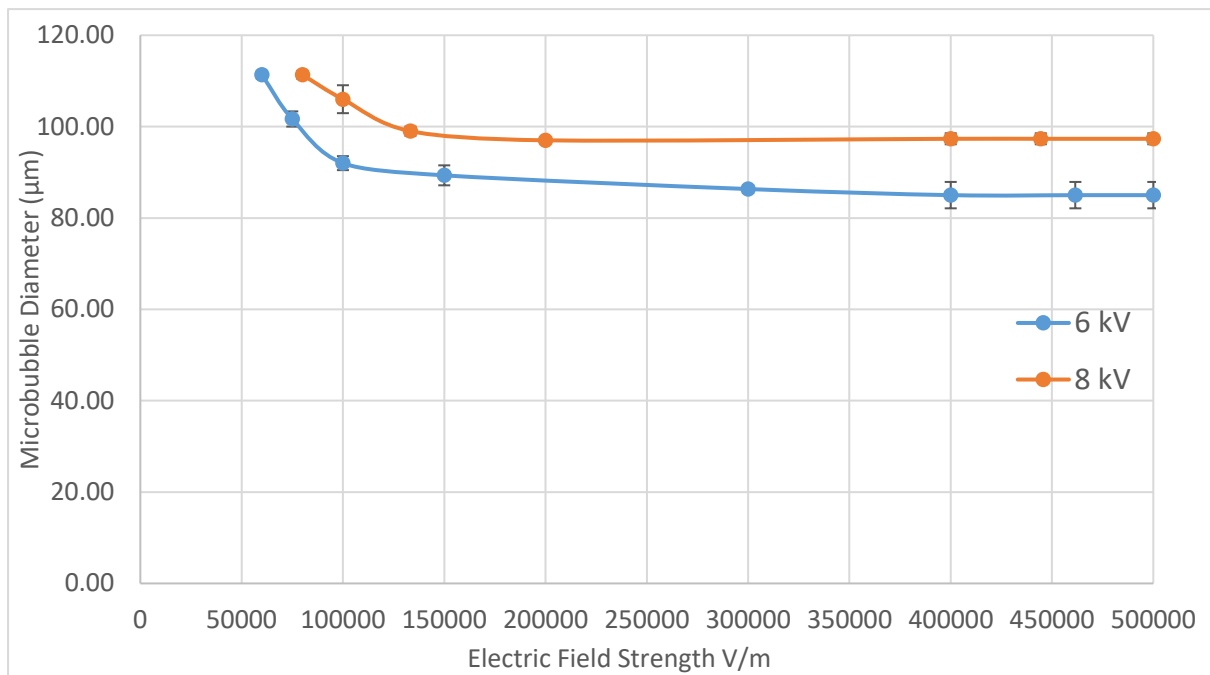
Figure 7: Graph summarising the effect of the electric field at 6kV DC and 8kV DC at 2kV AC P-P, 2 kHz for 10%wt. BSA Solution

Movassat et al.[31] modelled the oscillatory behaviour of a bubble when subjected to large vibrations. The bubble begins to deform, resulting in the formation of a dimple in its centre as shown in figure 8a. When this oscillatory force increases, the bubble undergoes break up. These authors suggested that this break-up is facilitated by a thin liquid jet that forms within the core of the bubble (figure 8b).
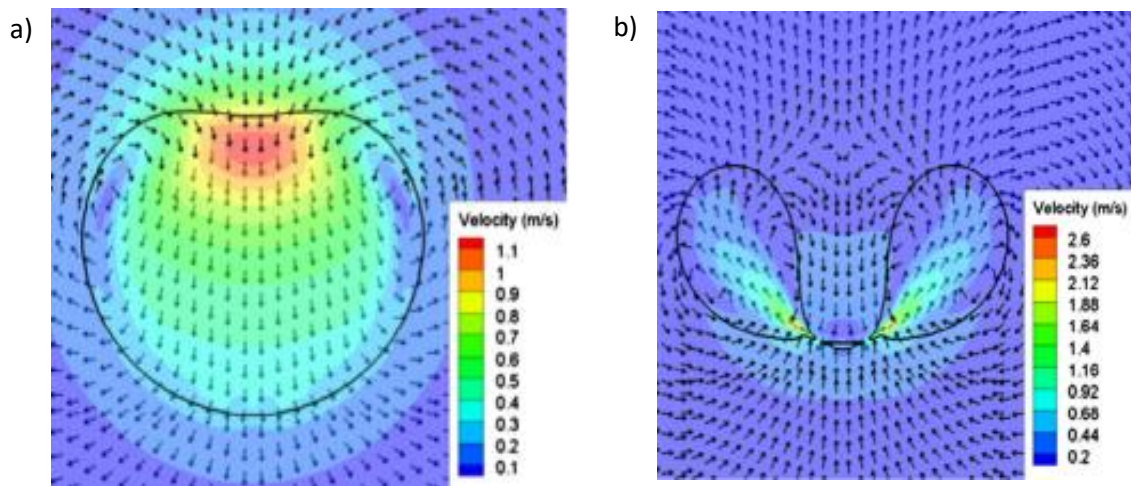

Figure 8: a) Cavitation of bubble resulting in the formation of a slight depression in the centre of the bubble b) a cut forms through the centre of the bubble due to increase in oscillatory force, the two halves are held together by a thin liquid jet (extracted from Movassat et al.) [1]

In bubble dynamics, the resistance to change in velocity (inertia) of the liquid penetrates towards the centre of the bubble, altering the bubble volume. Jagannathan et al. [33] added that when bubbles suspended in liquid are subjected to an acoustic vibration of specified frequencies, they experience

---

[1] Reprinted from Oscillation and breakup of a bubble under forced vibration, 54 , Mohammad Movassat, Nasser Ashgriz, Markus Bussmann, Oscillation and breakup of a bubble under forced vibration, Pages 211-219, Copyright (2015), with permission from Elsevier

variations in the surrounding pressure. They observed rapid fragmentation of bubbles at high frequencies as a result of the cavitation and subsequent deformation of the larger bubbles which is in accordance with the research conducted by Movassat et al. [31].

From figure 7, it can be observed that the greatest reduction in microbubble diameter was at 400,000 V/m. The ideal parameters for microbubble reduction obtained in the previous investigations, were incorporated for the next set of experiments using 10% wt BSA   BSA, Mx=100 µm and Dx= 400,000 V/m. The experiments were conducted at a constant applied AC voltage of 2kV $_{(P-P)}$ and varying the frequency between 1 kHz-10kHz at an applied DC voltage of 6kV. The corresponding optical micrographs obtained are presented in figure 9. It can be observed by incorporating the optimised parameters and steadily increasing the applied frequency further causes a reduction of 111±1µm to 18±2µm. These results are summarised in figure 10.
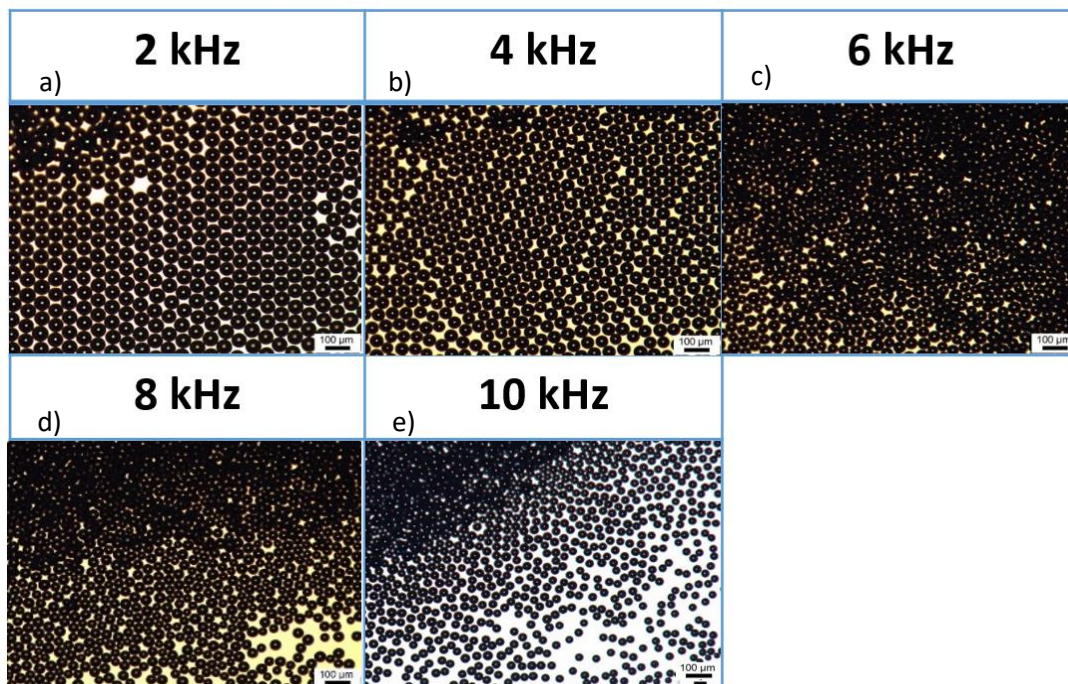

Figure 9: Optical Micrographs at 6kV at frequencies of a) 2 kHz b) 4kH c) 6kHz d) 8kHz e) and 10kHz

Developing a methodology to reduce microbubble diameter paves way to address the biomedical applications of microbubbles i.e. in ultrasound contrast agents and in targeted drug delivery which require microbubbles to range between 2-10µm in order to traverse through minor capillaries in the body and to avoid the risk of embolism[34].

There is similarity in the behaviour of the microbubbles observed in this work in comparison with other electrohydrodynamic procedures such as electrohydrodynamic forming. Doshi and Reneker[35]observed in their work on electrospinning, that the jet diameter decreased with increasing nozzle-to-collector distance displaying and inversely proportional relationship. Hekmati et al.[36] recorded that reducing the nozzle-to-collector distance also contributed to jet instability and an increase in the polydispersity of the fibres produced, this could be due to incomplete solvent evaporation and also the increase in the field strength when the applied electric field is constrained to a smaller gap, where the latter contributed to the formation of smaller bubbles in the research entailed in this manuscript.
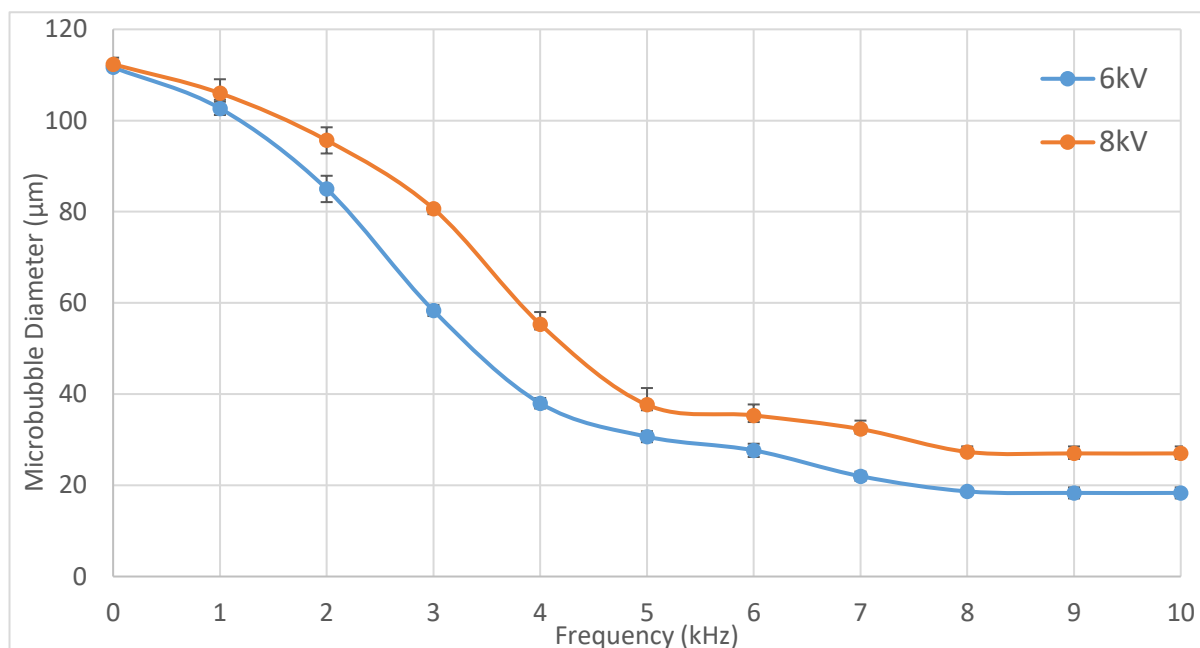
Figure 10 : Graph summarising the effect of frequency on microbubble diameter with optimised parameters of Mx= 20mm, Dx= 400 V/m, 2kV AC P-P at 6kV DC and 8kV DC

Henriques et al.[37] suggested that apart from incomplete solvent evaporation, larger nozzle-to-collector distances sustain weaker electric field strength. Ghelich et al.[38] recorded a similar occurrence of incomplete solvent evaporation as the aforementioned authors. At a distance of 80mm, fibres formed were not fine and residual fluid was present at the collector indicating incomplete solvent evaporation, increasing the distance to 100mm generated fine fibres without any influence on the fibre diameter from the sample collected at 80mm. However, further increasing the distance between the nozzle and collector to 150mm had a pronounced effect on fibre diameter increase owing to the reduction of electrostatic field strength hindering the stretching of the fibres. In this work, there was no specific attempt to study bubble stability as only a simple BSA-water model system was used, however the monodisperse microbubbles prepared were stable (I.e. no diameter range) for at least 60-90 minutes.

Conclusions

Two major lines of investigation were conducted in this work in order to understand additional factors that enable further control over microbubble size. Firstly, varying the Mx between the coaxially aligned channels had a pronounced effect in bubble size reduction, especially at Mx=100 . A decrease in bubble diameter from 128 ± 3µm to 71 ± 4µm was observed when 15% BSA was used as the continuous fluid medium. Bubble break up occurs when viscous shear overcomes the surface tension, as the Mx is reduced, the surface area of the junction region also reduces thus elevating the shear forces experienced at the junction, hence facilitating the break-up of bubbles into smaller bubbles. Finally, it was observed that constraining the electric field to a smaller area by decreasing Dx resulted in a reduction in microbubble diameter from 111 ± 1µm to 97 ± 2µm. This is due to an increase in electric field strength suggesting that very high voltages need not be utilised to facilitate bubble break-up, but constraining the electric field to a smaller region, can potentially promote bubble break-up as the effect of the electric field on the fluid stream is intensified. An optimised set-up employing the parameters from the previously discussed investigations enabled formation of microbubbles with diameters of 18 ± 2µm. The results achieved in this study suggest that a unique combination of

parameters can be selected to achieve particular bubble sizes to suit various applications. This novel apparatus presents a viable and innovative methodology to prepare monodisperse microbubbles with precision and provides the user with control over the bubble diameter and overall process.

References

1.   Minor, M.; Vingerhoeds, M. H.; Zoet, F. D.; De Wijk, R.; Van Aken, G. A., Preparation and sensory perception of fat-free foams – effect of matrix properties and level of aeration. *International Journal of Food Science & Technology* **2009,** *44* (4), 735-747.

2.   Campbell, G. M.; Mougeot, E., Creation and characterisation of aerated food products. *Trends in Food Science & Technology* **1999,** *10* (9), 283-296.

3.   Ahmad, B.; Stride, E.; Edirisinghe, M., Calcium Alginate Foams Prepared by a Microfluidic T-Junction System: Stability and Food Applications. *Food Bioprocess Technol* **2012,** *5* (7), 2848-2857.

4.   Shen, Y.; Longo, M. L.; Powell, R. L., Stability and rheological behavior of concentrated monodisperse food emulsifier coated microbubble suspensions. *Journal of Colloid and Interface Science* **2008,** *327* (1), 204-210.

5.   Jabesa, A.; Ghosh, P., Removal of diethyl phthalate from water by ozone microbubbles in a pilot plant. *Journal of Environmental Management* **2016,** *180*, 476-484.

6.   Wen, L. H.; Ismail, A. B.; Menon, P.; Saththasivam, J.; Thu, K.; Choon, N. K., Case studies of microbubbles in wastewater treatment. *Desalination and Water Treatment* **2011,** *30* (1-3), 10-16.

7.   Gwenaelle, M. P. O.; Jung, J.; Choi, Y.; Lee, S., Effect of microbubbles on microfiltration pretreatment for seawater reverse osmosis membrane. *Desalination* **2017,** *403*, 153-160.

8.   Al-mashhadani, M. K. H.; Wilkinson, S. J.; Zimmerman, W. B., Carbon dioxide rich microbubble acceleration of biogas production in anaerobic digestion. *Chemical Engineering Science* **2016,** *156*, 24-35.

9.   Hanotu, J.; Bandulasena, H. C. H.; Chiu, T. Y.; Zimmerman, W. B., Oil emulsion separation with fluidic oscillator generated microbubbles. *International Journal of Multiphase Flow* **2013,** *56*, 119-125.

10.   Liu, S.; Wang, Q.; Sun, T.; Wu, C.; Shi, Y., The effect of different types of micro-bubbles on the performance of the coagulation flotation process for coke waste-water. *Journal of Chemical Technology & Biotechnology* **2012,** *87* (2), 206-215.

11.   Liu, C.; Tanaka, H.; Ma, J.; Zhang, L.; Zhang, J.; Huang, X.; Matsuzawa, Y., Effect of microbubble and its generation process on mixed liquor properties of activated sludge using Shirasu porous glass (SPG) membrane system. *Water Research* **2012,** *46* (18), 6051-6058.

12.   Ten, S. T.; Hashim, U.; Gopinath, S. C. B.; Liu, W. W.; Foo, K. L.; Sam, S. T.; Rahman, S. F. A.; Voon, C. H.; Nordin, A. N., Highly sensitive Escherichia coli shear horizontal surface acoustic wave biosensor with silicon dioxide nanostructures. *Biosensors and Bioelectronics* **2017,** *93*, 146-154.

13.   Zhou, Y.; Seshia, A. A.; Hall, E. A. H. In *Microfluidics-based acoustic microbubble biosensor*, 2013 IEEE SENSORS, 3-6 Nov. 2013; 2013; pp 1-4.

14.   Parhizkar, M.; Edirisinghe, M.; Stride, E., Effect of operating conditions and liquid physical properties on the size of monodisperse microbubbles produced in a capillary embedded T-junction device. *Microfluid Nanofluid* **2013,** *14* (5), 797-808.

15.   Gupta, A.; Kumar, R., Effect of geometry on droplet formation in the squeezing regime in a microfluidic T-junction. *Microfluid Nanofluid* **2010,** *8* (6), 799-812.

16.   Fu, T.; Ma, Y.; Funfschilling, D.; Zhu, C.; Li, H. Z., Squeezing-to-dripping transition for bubble formation in a microfluidic T-junction. *Chemical Engineering Science* **2010,** *65* (12), 3739-3748.

17.   Wang, X.; Riaud, A.; Wang, K.; Luo, G., Pressure drop-based determination of dynamic interfacial tension of droplet generation process in T-junction microchannel. *Microfluid Nanofluid* **2015,** *18* (3), 503-512.

18.   Parhizkar, M.; Stride, E.; Edirisinghe, M., Preparation of monodisperse microbubbles using an integrated embedded capillary T-junction with electrohydrodynamic focusing. *Lab on a Chip* **2014,** *14* (14), 2437-2446.

19.   Jaworek, A.; Machowski, W.; Krupa, A.; Balachandran, W. In *Viscosity effect on EHD spraying using AC superimposed on DC electric field*, Industry Applications Conference, 2000. Conference Record of the 2000 IEEE, IEEE: 2000; pp 770-776.

20.   Balachandran, W.; Machowski, W.; Ahmad, C. N. In *Electrostatic atomisation of conducting liquids using AC superimposed on DC fields*, Industry Applications Society Annual Meeting, 1992., Conference Record of the 1992 IEEE, 4-9 Oct. 1992; 1992; pp 1369-1373 vol.2.

21.   Huneiti, Z.; Machowski, W.; Balachandran, W. In *Excitation of electrohydrodynamic surface waves on a conducting liquid jet employing AC field*, Industry Applications Conference, 1996. Thirty-First IAS Annual Meeting, IAS'96., Conference Record of the 1996 IEEE, IEEE: 1996; pp 1768-1774.

22.   Said, T.; Varadan, V. V. In *Variation of Cole-Cole model parameters with the complex permittivity of biological tissues*, Microwave Symposium Digest, 2009. MTT'09. IEEE MTT-S International, IEEE: 2009; pp 1445-1448.

23.   Kothandaraman, A.; Harker, A.; Ventikos, Y.; Edirisinghe, M., Novel Preparation of Monodisperse Microbubbles by Integrating Oscillating Electric Fields with Microfluidics. *Micromachines* **2018,** *9* (10), 497.

24.   Garstecki, P.; Fuerstman, M. J.; Stone, H. A.; Whitesides, G. M., Formation of droplets and bubbles in a microfluidic T-junction—scaling and mechanism of break-up. *Lab on a Chip* **2006,** *6* (3), 437-446.

25.   Baroud, C. N.; Gallaire, F.; Dangla, R., Dynamics of microfluidic droplets. *Lab on a Chip* **2010,** *10* (16), 2032-2045.

26.   Pancholi, K.; Stride, E.; Edirisinghe, M., Dynamics of bubble formation in highly viscous liquids. *Langmuir* **2008,** *24* (8), 4388-4393.

27.   Stride, E.; Edirisinghe, M., Novel microbubble preparation technologies. *Soft matter* **2008,** *4* (12), 2350-2359.

28.   Ahmad, Z.; Zhang, H. B.; Farook, U.; Edirisinghe, M.; Stride, E.; Colombo, P., Generation of multilayered structures for biomedical applications using a novel tri-needle coaxial device and electrohydrodynamic flow. *Journal of the Royal Society Interface* **2008,** *5* (27), 1255-1261.

29.   Zeleny, J., The Electrical Discharge from Liquid Points, and a Hydrostatic Method of Measuring the Electric Intensity at Their Surfaces. *Physical Review* **1914,** *3* (2), 69-91.

30.   Sarkar, S.; Deevi, S.; Tepper, G., Biased AC electrospinning of aligned polymer nanofibers. *Macromolecular rapid communications* **2007,** *28* (9), 1034-1039.

31.   Movassat, M.; Ashgriz, N.; Bussmann, M., Oscillation and breakup of a bubble under forced vibration. *International Journal of Heat and Fluid Flow* **2015,** *54* (0), 211-219.

32.   Vonnegut, B.; Neubauer, R. L., Production of monodisperse liquid particles by electrical atomization. *Journal of Colloid Science* **1952,** *7* (6), 616-622.

33.   Jagannathan, T. K.; Nagarajan, R.; Ramamurthi, K., Effect of ultrasound on bubble breakup within the mixing chamber of an effervescent atomizer. *Chemical Engineering and Processing: Process Intensification* **2011,** *50* (3), 305-315.

34.   Farook, U.; Stride, E.; Edirisinghe, M. J.; Moaleji, R., Microbubbling by co-axial electrohydrodynamic atomization. *Medical & Biological Engineering & Computing* **2007,** *45* (8), 781-789.

35.   Doshi, J.; Reneker, D. H. In *Electrospinning process and applications of electrospun fibers*, Industry Applications Society Annual Meeting, 1993., Conference Record of the 1993 IEEE, IEEE: 1993; pp 1698-1703.

36.   Hekmati, A. H.; Rashidi, A.; Ghazisaeidi, R.; Drean, J.-Y., Effect of needle length, electrospinning distance, and solution concentration on morphological properties of polyamide-6 electrospun nanowebs. *Textile Research Journal* **2013**, 0040517512471746.

37.   Henriques, C.; Vidinha, R.; Botequim, D.; Borges, J.; Silva, J., A systematic study of solution and processing parameters on nanofiber morphology using a new electrospinning apparatus. *Journal of nanoscience and nanotechnology* **2009,** *9* (6), 3535-3545.

38.   Ghelich, R.; Keyanpour-Rad, M.; Yuzbashi, A., Study on morphology and size distribution of electrospun NiO–GDC composite nanofibers. *J. Eng. Fibers Fabr* **2013**.